ACS OMEGA

http://pubs.acs.org/journal/acsodf

Article

Novel Heteroleptic Tin(II) Complexes Capable of Forming SnO and SnO_2 Thin Films Depending on Conditions Using Chemical Solution Deposition

Seong Ho Han, Raphael Edem Agbenyeke, Ga Yeon Lee, Bo Keun Park, Chang Gyoun Kim, Taeyong Eom, Seung Uk Son, Jeong Hwan Han, Ji Yeon Ryu, and Taek-Mo Chung*

Cite This: *ACS Omega* 2022, 7, 1232−1243

Read Online

ACCESS | Metrics & More | Article Recommendations | Supporting Information

ABSTRACT: A new heteroleptic complex series of tin was synthesized by the salt metathesis reaction of SnX_2 (X = Cl, Br, and I) with aminoalkoxide and various *N*-alkoxy-functionalized carboxamide ligands. The complexes, $[ClSn(dmamp)]_2$ (**1**), $[BrSn(dmamp)]_2$ (**2**), and $[ISn(dmamp)]_2$ (**3**), were prepared from the salt metathesis reaction of SnX_2 with one equivalent of dmamp; $[Sn(dmamp)(empa)]_2$ (**4**), $[Sn(dmamp)(mdpa)]_2$ (**5**), and $[Sn(dmamp)(edpa)]_2$ (**6**) were prepared via the salt metathesis reaction using complex **2** with one equivalent of *N*-alkoxy-functionalized carboxamide ligand. Complexes **1**−**5** displayed dimeric molecular structures with tin metal centers interconnected by μ_2−O bonding via the alkoxy oxygen atom. The molecular structures of complexes **1**−**5** showed distorted trigonal bipyramidal geometries with lone pair electrons in the equatorial position. Using complex **6** as a tin precursor, SnO_x films were deposited by chemical solution deposition (CSD) and subsequent post-deposition annealing (PDA) at high temperatures. SnO and SnO_2 films were selectively obtained under controlled PDA atmospheres of argon and oxygen, respectively. The SnO films featured a tetragonal romarchite structure with high crystallinity and a preferred growth orientation along the (101) plane. They also exhibited a lower transmittance of >52% at 400 nm due to an optical band gap of 2.9 eV. In contrast, the SnO_2 films exhibited a tetragonal cassiterite crystal structure and an extremely high transmittance of >97% at 400 nm was observed with an optical band gap of 3.6 eV.

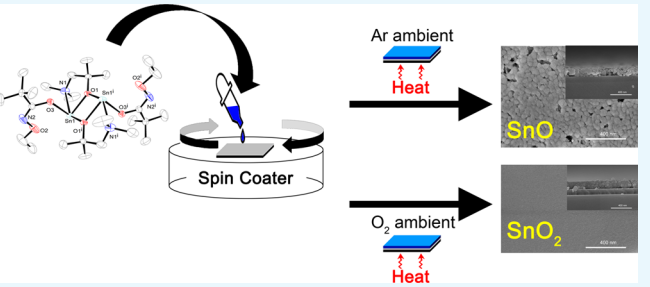

INTRODUCTION

Tin oxide (SnO_2) is an attractive n-type oxide with a wide band gap of 3.62 eV.[1] Additionally, it is chemically stable, has high abrasion resistance, and displays over 80% optical transparency in visible and near-infrared regions. Especially, SnO_2 has useful electrical properties with high electrical conductivity owing to its electron concentration levels of 10^{14}−10^{21} cm^{-3}. The formation of excess electrons is attributed to the presence of intrinsic point defects such as oxygen vacancies or Sn interstitials in SnO_2.[2−4] With these properties, SnO_2 has been applied to gas sensors that detect CO_2 and H_2,[5] photosensors,[6] catalytic support materials,[7] solar cells,[8] solid-state chemical sensors,[9,10] and transparent conducting oxide applications in photovoltaics and flat panels.[11] Meanwhile, p-type transparent oxide is a field that should essentially be studied to develop transparent and photo devices such as p−n junctions and complementary metal-oxide semiconductor (CMOS) architectures with n-type transparent oxide materials.[12] Compared to n-type oxide materials such as ZnO, SnO_2, ZnSnO, InGaZnO, WO_3, etc., p-type materials such as SnO, Cu_2O, and N-doped ZnO were rarely explored. Among the various p-type oxide, SnO (tin(II) monoxide) has attracted great interest due to a wide optical band gap of 2.7−3.0 eV and high Hall mobility of ∼18.71 $cm^2/(V{\cdot}s)$,[13] which enables the realization of transparent CMOS devices. Recently, it was reported that SnO based thin film transistor (TFT) showed high field-effect mobility of ∼6.75 $cm^2/(V{\cdot}s)$.[14]

Growth of SnO_x thin films has been demonstrated by the different deposition methods such as physical vapor deposition (PVD),[15−18] chemical vapor deposition (CVD),[19−22] atomic layer deposition (ALD),[23,24] and chemical solution deposition (CSD).[25] To selectively achieve the n-type SnO_2 and p-type SnO films, controlling the oxidation state of tin to be either +4 or +2 is essential by engineering the process conditions such as oxygen partial pressure and oxygen source.[26,27] Authors reported that SnO and SnO_2 phases are deposited by ALD

Received: October 18, 2021
Accepted: December 17, 2021
Published: December 29, 2021

Scheme 1. Synthesis of Complexes 1−6

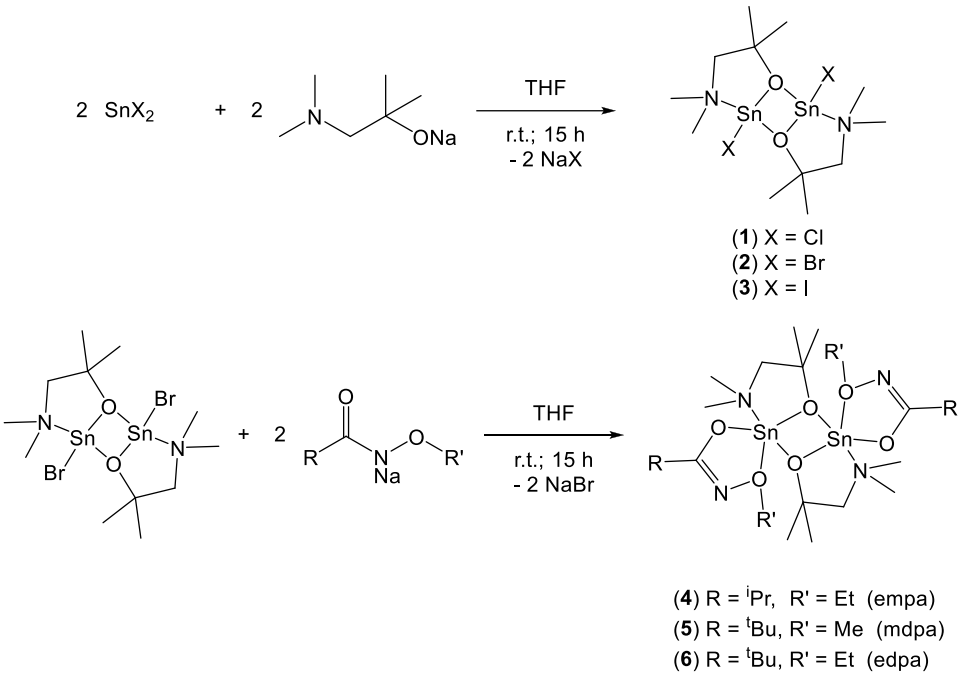

using a novel Sn(II) precursor, $Sn(dmamp)_2$ where dmamp is 1-dimethylamino-2-methyl-2-propoxide, in combination with H_2O and O_2 plasma, respectively.[27]

Various Sn(II) precursors have been used to deposit tin oxide (SnO and SnO_2), including $SnCl_2$,[28] Sn(tbba) (tbba = *N2,N3*-di-tert-butyl-butane-2,3-diamide),[29] $Sn(dmamp)_2$,[27,30] $Sn(acac)_2$ (acac = acetylacetonate),[31,32] $[Sn\{OC(NMe_2)\text{-}N^tBu\}_2]$,[22] and $Sn(btsa)_2$ (btsa = bis(trimethylsilyl)amide).[33] Widely known precursors were used to deposit Sn-based films, which have advantages such as low vapor pressure and decomposition of ligands during deposition.[34]

In this study, we demonstrate the synthesis and characterization of novel tin(II) precursors with a combination of 1-dimethylamino-2-methyl-2-propoxide (dmamp) and various *N*-alkoxy-functionalized carboxamides such as *N*-ethoxy-2-methylpropanamide (empa), *N*-methoxy-2,2-dimethylpropanamide (mdpa), and *N*-ethoxy-2,2-dimethylpropanamide (edpa). All complexes were characterized using nuclear magnetic resonance (NMR), Fourier-transform infrared spectroscopy (FT-IR), elemental analysis, X-ray crystallography, and thermogravimetric analysis (TGA). Using complex **6** as a tin precursor, SnO_x films were deposited by chemical solution deposition (CSD) and subsequent post-deposition annealing (PDA) at high temperatures. The SnO and SnO_2 films were selectively obtained under controlled PDA atmospheres of argon and oxygen, respectively.

RESULTS AND DISCUSSION

Synthesis. Novel tin complexes were synthesized using tin halide as the starting material by controlled salt metathesis reactions, as shown in Scheme 1.

In the first step, tin halide ($SnCl_2$, $SnBr_2$, and SnI_2) in THF was mixed with 1 equivalent of Na(dmamp) at room temperature. $[ClSn(dmamp)]_2$ (**1**), $[BrSn(dmamp)]_2$ (**2**), and $[ISn(dmamp)]_2$ (**3**) were isolated through extraction with THF. To prepare new heteroleptic tin complexes $[Sn(dmamp)(N\text{-alkoxy carboxamide})]_2$, three $[Sn(dmamp)\text{-}(halide)]_2$ were used as the starting materials. Among them, Sn(dmamp)Br was selected as the final starting material because it gave the best reaction product yields under the optimum reaction conditions. In the second step, **2** reacted with sodium *N*-alkoxy carboxamides such as Na(empa), Na(mdpa), and Na(edpa) in THF solution at room temperature in an argon-filled glovebox. The products, $[Sn(dmamp)\text{-}(empa)]_2$ (**4**), $[Sn(dmamp)(mdpa)]_2$ (**5**), and $[Sn(dmamp)\text{-}(edpa)]_2$ (**6**), were extracted with hexane and recrystallized at room temperature by slow evaporation to provide good to excellent yields. All complexes synthesized in this work were highly soluble in common organic solvents such as hexane, toluene, THF, and diethyl ether. Furthermore, all complexes were quite stable under inert conditions such as a nitrogen or an argon atmosphere.

NMR Spectral Analysis. All compounds were analyzed via NMR spectroscopy, and benzene-d_6 and chloroform-*d* were used as a solvent and reference at room temperature, respectively.

In the ^1H NMR spectra, the $OC(CH_3)_2$ group of the dmamp ligand of all complexes showed singlet resonances at 1.49 ppm for **1**, 1.49 ppm for **2**, 1.48 ppm for **3**, 1.44 ppm for **4**, 1.43 ppm for **5**, and 1.42 ppm for **6**, respectively; this showed a clean downfield shift compared to the free dmampH signal at 1.13 ppm. The $N(CH_3)_2$ group of the dmamp ligand exhibited singlet resonances at 1.79 and 2.20 ppm for **1**, 2.01 ppm for **2**, 2.05 ppm for **3**, 2.06 ppm for **4**, 2.02 ppm for **5**, and 2.05 ppm for **6**, respectively; these results exhibited a clean upfield shift compared to the free dmampH signal at 2.11 ppm, except complex **1**. Additionally, the NCH_2CO group of the dmamp ligand displayed singlet resonances at 1.92 and 2.49 ppm for **1**, 2.24 ppm for **2**, 2.31 ppm for **3**, 2.20 ppm for **4**, 2.21 ppm for **5**, and 2.21 ppm for **6**, respectively. These results displayed a clean upfield shift compared to the free dmampH resonance at 2.03 ppm, except complex **1**. Interestingly, the ^1H NMR spectra of compound **1** showed that methyl protons

https://doi.org/10.1021/acsomega.1c05744
ACS Omega 2022, 7, 1232−1243

Table 1. Crystallographic Parameters of Complexes 1−5

compound	1	2	3	4	5
empirical formula	$C_{12}H_{28}Cl_2N_2O_2Sn_2$	$C_{12}H_{28}Br_2N_2O_2Sn_2$	$C_{12}H_{28}I_2N_2O_2Sn_2$	$C_{24}H_{52}N_4O_6Sn_2$	$C_{24}H_{52}N_4O_6Sn_2$
formula weight	270.32	629.56	361.77	730.08	730.08
T/K	100(1)	296(1)	100(1)	100(1)	100(1)
crystal system	monoclinic	monoclinic	triclinic	triclinic	triclinic
space group	P2(1)/n	P2(1)/c	P-1	P-1	P-1
a (Å)	7.6737(4)	14.699(6)	7.7781(12)	8.8721(2)	8.114(2)
b (Å)	10.8936(5)	11.931(5)	7.9123(13)	13.1408(2)	10.026(3)
c (Å)	11.9476(6)	12.435(6)	9.4845(15)	14.4809(2)	11.148(3)
α (°)	90	90	89.514(7)	77.1780(10)	71.863(12)
β (°)	105.626(2)	111.161(18)	78.657(7)	79.0910(10)	75.559(11)
γ (°)	90	90	70.302(7)	82.6400(10)	78.093(12)
V (Å ^{3})	961.84(8)	2033.7(15)	537.75(15)	1609.88(5)	826.4(4)
Z	4	4	2	2	1
density(g/cm^{-3})	1.867	2.056	2.234	1.506	1.467
absorption coefficient	2.877	6.388	5.196	1.590	1.549
F(000)	528	1200	336	744	372
crystal size (mm^3)	0.40 × 0.10 × 0.09	0.38 × 0.20 × 0.14	0.10 × 0.10 × 0.08	0.18 × 0.10 × 0.06	0.26 × 0.18 × 0.06
theta range for data collection (°)	2.57−28.35	1.49−28.36	2.19−26.00	1.46−26.73	1.96−26.00
index ranges	−10 ≤ h≤ 9, 0 ≤ k ≤ 14, 0 ≤ l ≤15	0 ≤ h ≤ 19, −15 ≤ k ≤ 0, −16 ≤ l ≤15	−9 ≤ h ≤9, −9 ≤ k ≤ 9, 0 ≤ l ≤ 11	−10 ≤ h ≤ 11, −15 ≤ k ≤ 16, 0 ≤ l ≤ 18	−9 ≤ h ≤ 9, −11 ≤ k ≤ 12, 0 ≤ l ≤ 13
reflections collected	2359	5036	2048	4238	3200
independent reflections	2359 [R(int) = 0.0000]	5036 [R(int) = 0.0000]	2048 [R(int) = 0.0000]	6829 [R(int) = 0.0000]	3200 [R(int) = 0.0000]
goodness-of-fit on F^2	1.269	1.090	1.074	1.033	1.076
R[a][I > 2σ(I)]	0.0232	0.0321	0.0243	0.0207	0.0327
wR2[b]	0.0561	0.0906	0.0608	0.0480	0.0819

[a]R = (∑||Fol-|Fc||)/∑|Fol. [b]wR2 = [∑ω(Fo2-Fc2)2/∑ω(Fo2)2]1/2.

(1.79 and 2.19 ppm) and methylene protons (1.92 and 2.49 ppm) of the dmamp ligand resonated as two singlets.

In **4**, part of the empa ligand showed signals at δ = 1.35 (OCH_2CH_3 and $CH(CH_3)_2$), 2.81 ($CH(CH_3)_2$), and 4.18 (OCH_2CH_3) ppm; these shifted downfield from those of free ligand of empaH (1.14, 2.62, and 3.95 ppm). For the mdpa moiety of **5**, the signals of $OCC(CH_3)_3$ and OCH_3 at δ = 1.48 and 3.82 ppm, respectively, shifted downfield compared to the free mdpaH ligand (1.09 and 3.59 ppm). For **6**, part of the edpa signals appeared at δ = 1.32, 1.46, and 4.16 ppm; these represented a downfield shift from the free edpaH ligand (1.10, 1.16, and 3.84 ppm).

Boyle and co-workers synthesized two 4-coordinated tin(II) alkoxide complexes, $[Sn(\mu\text{-}OR)_2]_\infty$ (R = 2-methylphenolate and 2-isopropylphenolate), which showed major resonances at −412 and −429 ppm in the $^{119}Sn\{^1H\}$ NMR spectra, respectively.[35] Moreover, Linda and co-workers prepared 4-coordinated tin(II) compounds $K_2[Sn^{II}(pin^F)_2]$ and $[(15C5)_2K]_2[Sn^{II}(pin^F)_2]$ (pin^F = dianionic perfluoropinacolate) with major signals at −435 and −501 ppm in the ^{119}Sn NMR spectra.[36] The ^{119}Sn $\{^1H\}$ NMR spectra of complexes **4**−**6** showed single resonances of −414, −417, and −418 ppm, respectively. These $^{119}Sn\{^1H\}$ NMR spectra for complexes **4**−**6** are consistent with previously reported complexes.[35,36]

Crystal Structures. X-ray quality crystals were obtained by slow evaporation of a saturated THF solution for complexes **1**−**3** and saturated hexane for complexes **4**−**5**. Complexes **1** and **2** crystallized in the monoclinic space group, whereas complexes **3**−**5** crystallized in the triclinic space group (Table 1). All complexes formed essentially centrosymmetric dimers with aminoalkoxide oxygen bridging the two metal centers in the complexes via μ_2−O bonding, similar to the bonding pattern of other metal complexes (Mg, Sr, In, Co, Zn) containing aminoalkoxide reported previously.[37−43] In the case of compounds **3**−**5**, they are also located on crystallographic centers of inversion. All structures have a four-membered Sn_2O_2 core ring. In complexes **1**−**3**, the tin metal in each was bonded to one terminal halide, one amino group, and two bridging alkoxide groups with lone pair electrons; the metal exhibited seesaw geometries where the lone pair electrons on the central metal are in an equatorial position (as shown in Figures 1−3). The aminoalkoxide ligand, dmamp is bound to tin as a bidentate ligand and forms a 5-membered ring composed of Sn−N−C−C−O. Selected bond lengths and bond angles of complexes **1**−**3** are listed in Table 2.

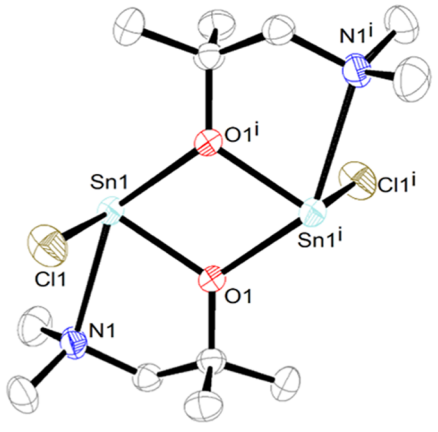

Figure 1. Crystal structure of $[ClSn(dmamp)]_2$ (**1**).

https://doi.org/10.1021/acsomega.1c05744
ACS Omega 2022, 7, 1232−1243

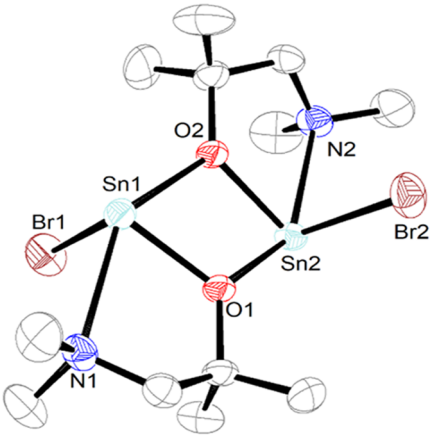

Figure 2. Crystal structure of $[BrSn(dmamp)]_2$ (**2**).

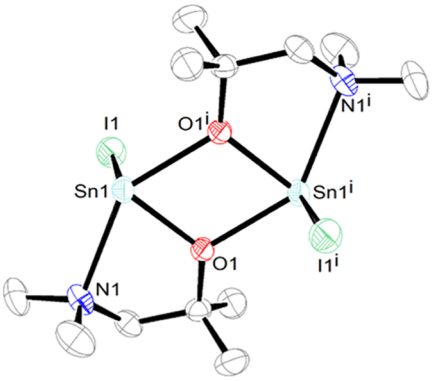

Figure 3. Crystal structure of $[ISn(dmamp)]_2$ (**3**).

The bond lengths between tin and ionic oxygen atom (2.107(2) (**1**), 2.092(2) (**2**), and 2.092(2) Å (**3**)) in compound **1**−**3** were shorter than those of tin-dative bonding oxygen (2.276(2) (**1**), 2.296(2) (**2**), and 2.299(2) Å (**3**)) by 0.169−0.207 Å. Sn−O and Sn ← O bond lengths of compounds were similar to those of $[ClSn(dmae)]_2$ (2.104(3) and 2.240(3) Å) (where dmae = 2-dimethylaminoethoxide).[44] Also, Sn ← N coordination bond lengths of complexes **1**−**3** are 2.535(3), 2.558(3), and 2.487(3) Å, respectively, which are almost the same as that of $[ClSn(dmae)]_2$ (2.499(4) Å). The Sn−Cl bond length of compound **1** was 2.4816 Å which was similar to that of $[ClSn(dmae)]_2$ (2.473 Å).[44] The Sn−Br bond length of complex **2** was 2.6526(11) Å which was similar to that of SnCpBr(dip) (where dip = diisopropylcyclohexane) (2.691 Å).[45] The Sn−I bond length of complex **3** was 2.8951(6) Å which was longer than that of $[L^1SnI_2]\cdot[OTf]_2$ (2.6779 Å) (where L^1 = tris(1-ethyl-benzoimidazol-2-ylmethyl)amine).[46] The Sn···Sn distances within the Sn_2O_2 cores were 3.5978(4) (**1**), 3.5616(16) (**2**), and 3.5897(6) Å (**3**). The bite angles of O−Sn−N were 73.96(8) (**1**), 73.84(9) (**2**), and 72.28(10)° (**3**), which were close to the ideal degree (72°). In these complexes, the oxygen atom of the neighboring dmamp ligand ($O1^i$) and the nitrogen atom of the dmamp ligand (N1) were situated in axial positions with $O1^i$−Sn1−N1 bond angles of 142.56(8) (**1**), 143.63(8) (**2**), and 142.45(9)° (**3**), respectively. The oxygen atom of the dmamp ligand (O1), halide (Cl, Br, and I), and lone pair electrons of tin occupied the equatorial sites around the tin metal. The atoms of equatorial sites were located especially far from the lone pair electrons. The O1−Sn1−X angles of complexes **1**−**3** were 98.46(6), 98.17(6), and 93.01(6)°, respectively, which demonstrated that the equatorial site expected the lone pair electrons.

In complexes **4**−**5**, each tin metal was bonded to one *N*-alkoxy carboxamide, one amine group, and two bridging alkoxides with lone pair electrons. These tin metals showed distorted trigonal bipyramidal geometries, including lone pair electrons (shown in Figures 4 and 5). Similar to **1**−**3**, dmamp

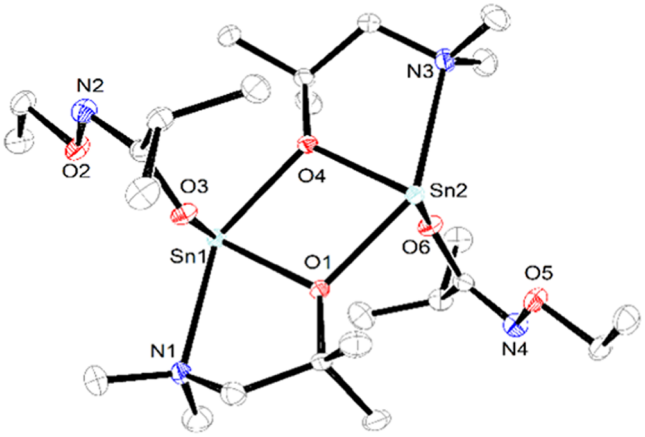

Figure 4. Crystal structure of $[Sn(dmamp)(empa)]_2$ (**4**).

Table 2. Selected Bond Lengths (Å) and Bond Angles (°) for Complexes 1−3

$[ClSn(dmamp)]_2$ (**1**)		$[BrSn(dmamp)]_2$ (**2**)		$[ISn(dmamp)]_2$ (**3**)	
Bond Lengths (Å)					
Sn1-O1	2.107(2)	Sn1-O1	2.092(2)	Sn1-O1	2.092(2)
Sn1-$O1^i$	2.276(2)	Sn1-O2	2.296(2)	Sn1-$O1^i$	2.299(2)
Sn1-N1	2.535(3)	Sn1-N1	2.558(3)	Sn1-N1	2.487(3)
Sn1-Cl1	2.4816(8)	Sn1-Br1	2.6526(11)	Sn1-I1	2.8951(6)
Sn1···$Sn1^i$	3.5978(4)	Sn1···Sn2	3.5616(16)	Sn1···$Sn1^i$	3.5897(6)
Bond Angles (°)					
O1-Sn1-$O1^i$	69.72(9)	O1-Sn1-O2	70.30(8)	O1-Sn1-$O1^i$	70.42(10)
O1-Sn1-N1	73.96(8)	O1-Sn1-N1	73.84(9)	O1-Sn1-N1	72.28(10)
O1-Sn1-Cl1	98.46(6)	O1-Sn1-Br1	98.17(6)	O1-Sn1-I1	93.01(6)
$O1^i$-Sn1-N1	142.56(8)	O2-Sn1-N1	143.63(8)	$O1^i$-Sn1-N1	142.45(9)
$O1^i$-Sn1-Cl1	89.39(6)	O2-Sn1-Br1	89.98(7)	$O1^i$-Sn1-I1	93.95(6)
N1-Sn1-Cl1	87.13(6)	N1-Sn1-Br1	89.27(7)	N1-Sn1-I1	92.10(7)
Sn1-O1-$Sn1^i$	110.28(9)	Sn1-O1-Sn2	108.37(9)	Sn1-O1-$Sn1^i$	109.58(10)

https://doi.org/10.1021/acsomega.1c05744
ACS Omega 2022, 7, 1232−1243

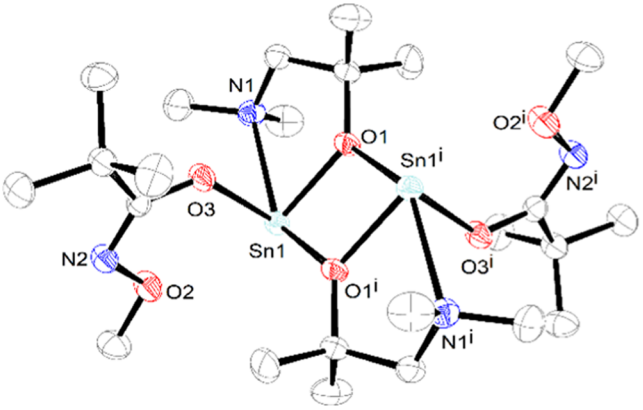

Figure 5. Crystal structure of [Sn(dmamp)(mdpa)]$_2$ (**5**).

in complexes **4**−**5** was bound to tin as a bidentate ligand and formed a 5-membered ring consisting of Sn−N−C−C−O. Additionally, the *N*-alkoxy carboxamide ligand was bound to the tin metal. Selected bond lengths and bond angles of complexes **4**−**5** are listed in Table 3. The bond lengths between tin and the ionic oxygen atom of the dmamp ligand (2.1396(13) (**4**) and 2.128(3) Å (**5**)) in compounds **4**−**5** were shorter than those of tin-dative bonding oxygen of the dmamp ligand (2.2800(12) (**4**) and 2.265(3) Å (**5**)) by 0.140 and 0.137 Å. Sn−O and Sn ← O bond lengths of compounds were (2.128(3) and 2.265(3) Å) similar to those of [ClSn(dmae)]$_2$ (2.104(3) and 2.240(3) Å).[44] Also, Sn ← N coordination bond lengths of complexes **4**−**5** are 2.4777(17) and 2.540(3) Å, respectively, which are similar to that of [ClSn(dmae)]$_2$ (2.499(4) Å). The bond lengths between the tin 1 and oxygen atom of the *N*-alkoxy carboxamide ligand (2.1035(14), 2.121(2) Å) in compounds **4**−**5** were similar to that of the reported Sn(*N*-alkoxy carboxamide)$_2$ (2.099(2) Å).[47] The distance of Sn1−O2 were 2.8789(14) (**4**) and 2.733(28) Å (**5**); these were significantly longer distances compared to the general Sn−O bond. The Sn···Sn distances within the Sn_2O_2 cores were 3.5813(2) (**4**) and 3.5594(9) Å (**5**). The bite angles of the dmamp moiety were 72.44(5) (**4**) and 72.64(10)° (**5**), respectively, which were close to the ideal pentagon degree (72°). In these complexes, the oxygen atom of the neighboring dmamp ligand (O4, O1^{i}) and the nitrogen atom of the dmamp ligand (N1) were situated in axial positions with (O4, O1^{i})−Sn−N1 bond angles of 142.69(5) (**4**), and 143.21(10)° (**5**), respectively. The oxygen atom of the dmamp ligand (O1), *N*-alkoxy carboxamide ligand (O3), and lone pair electrons of tin occupied the equatorial sites around the tin metal. The atoms were located especially far from the lone pair electrons.

Thermogravimetric Analysis. The TGA trace shown in Figure 6 clearly shows thermal decomposition of compounds

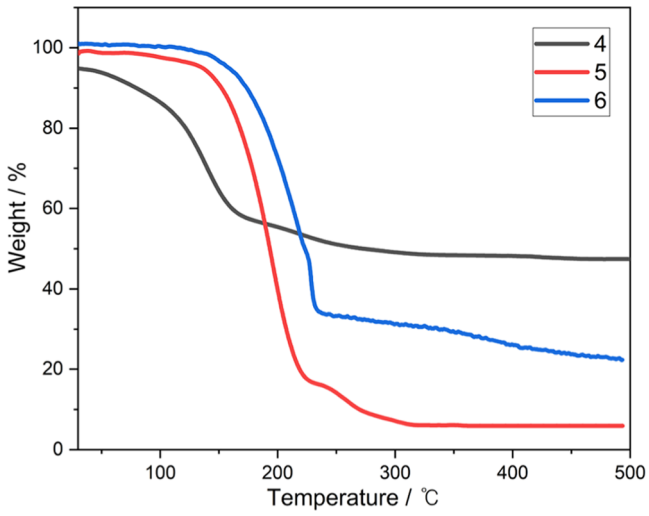

Figure 6. TGA plot of complexes **4**−**6**. Black (**4**), red (**5**), and blue (**6**).

4−**6** below 500 °C. The samples were prepared inside an argon-filled glovebox under a constant flow of nitrogen to minimize air contact. The TGA plot of complex **4** showed the main weight loss at 50−172 °C; the final residue was 47%, which was likely comprised of SnO_2, although the residue was more than the calculated value of SnO_2 (41%). Complex **5** displayed the main weight loss from 118−220 °C and the final residue was 6%, which indicated that the thermal decomposition and evaporation of the compound occurred during TGA. Moreover, the TGA curve of complex **6** showed the main weight loss at 123−235 °C with 22% residue, which was less than that calculated for the Sn metal (31%). All complexes

Table 3. Selected Bond Lengths (Å) and Bond Angles (°) of Complexes 4−5

	[Sn(dmamp)(empa)]$_2$ (**4**)			[Sn(dmamp)(mdpa)]$_2$ (**5**)	
		Bond Lengths (Å)			
Sn1-O1	2.1396(13)	Sn2-O4	2.1337(13)	Sn1-O1	2.128(3)
Sn1···O2	2.8789(14)	Sn2-O6	2.1033(14)	Sn1···O2	2.733(28)
Sn1-O3	2.1035(14)	Sn2-O1	2.2815(12)	Sn1-O3	2.121(2)
Sn1-O1^{i}	2.2800(12)	Sn2-N3	2.5691(17)	Sn1-O1^{i}	2.265(3)
Sn1-N1	2.4777(17)			Sn1-N1	2.540(3)
Sn1···Sn1^{i}	3.5813(2)			Sn1···Sn1^{i}	3.5594(9)
		Bond Angles (°)			
O1-Sn1-O3	83.91(5)	O4-Sn2-O6	87.51(5)	O1-Sn1-O3	83.55(10)
O1-Sn1-O4	71.58(5)	O4-Sn2-O1	71.65(5)	O1-Sn1-O1^{i}	71.78(9)
O1-Sn1-N1	72.44(5)	O4-Sn2-N3	72.70(5)	O1-Sn1-N1	72.64(10)
O3-Sn1-O4	86.02(5)	O6-Sn2-O1	86.11(5)	O3-Sn1-O1^{i}	86.01(10)
O3-Sn1-N1	80.71(5)	O6-Sn2-N3	82.61(5)	O3-Sn1-N1	81.02(11)
O4-Sn1-N1	142.69(5)	O1-Sn2-N3	142.96(5)	O1^{i}-Sn1-N1	143.21(10)
Sn1-O1-Sn2	108.16(6)	Sn1-O4-Sn2	108.42(6)	Sn1-O1-Sn1^{i}	108.22(9)

https://doi.org/10.1021/acsomega.1c05744
ACS Omega 2022, 7, 1232−1243

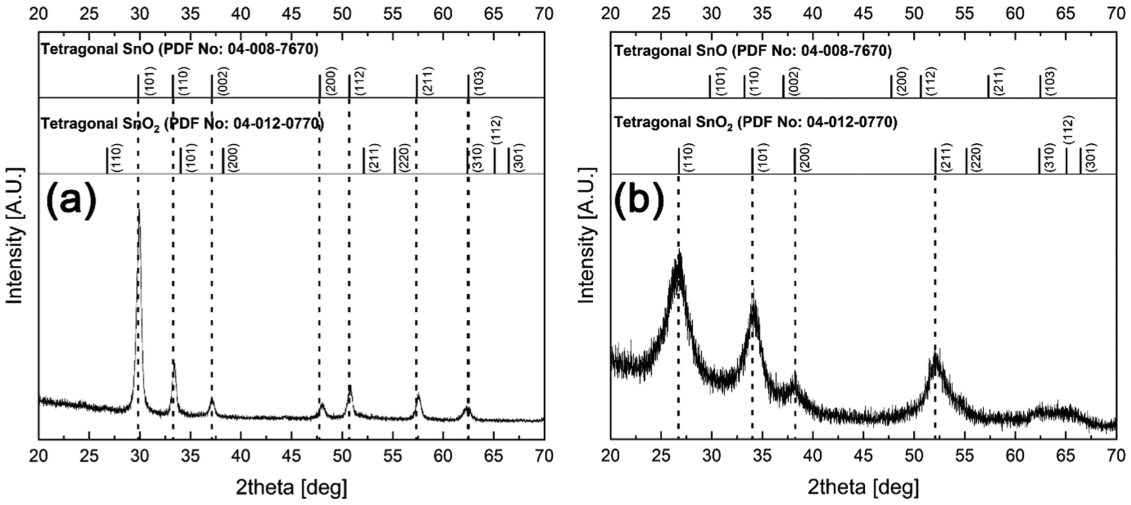

Figure 7. GAXRD patterns for SnO_x films annealed in (a) argon and (b) oxygen.

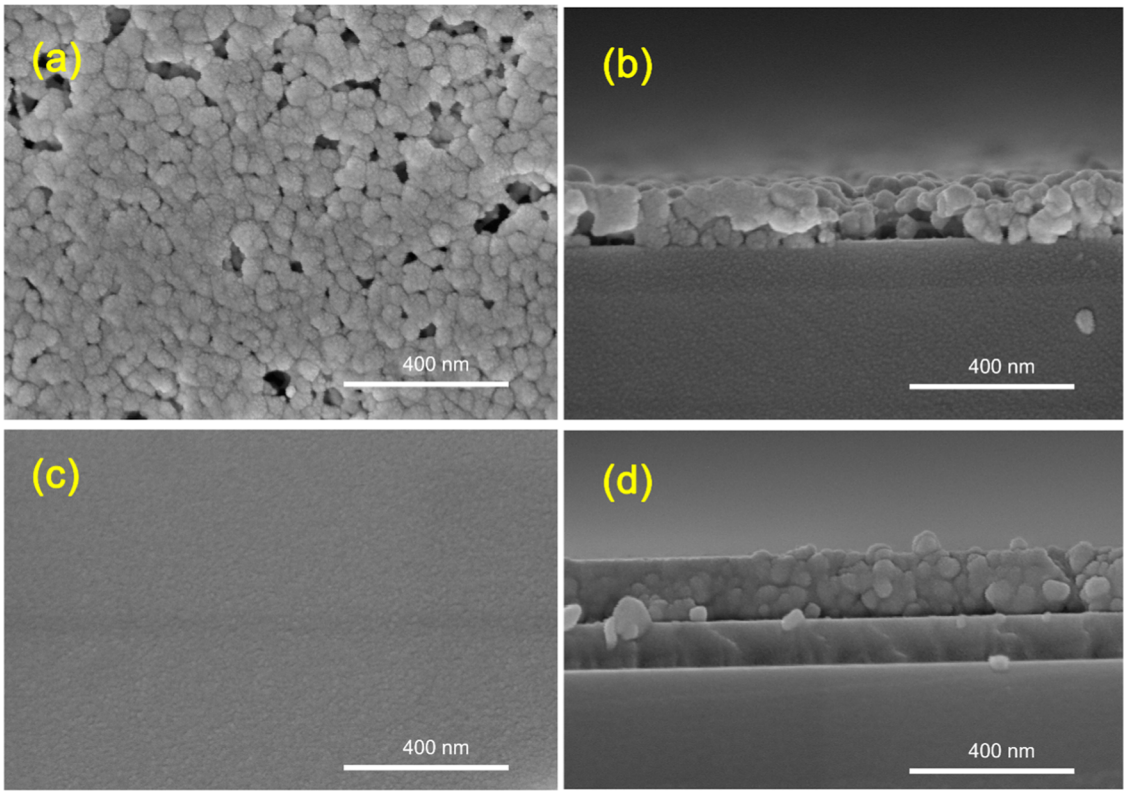

Figure 8. FE-SEM images: (a) Plane view and (b) cross-sectional images of the SnO film. FE-SEM images: (c) Plane view and (d) cross-sectional images of the SnO_2 film.

displayed decomposition during TGA experiments owing to their thermal instability.

Deposition and Properties of SnO and SnO_2 Using Complex (6). The TGA plots in Figure 6 showed that the thermal instability of compounds **4**–**6** led to their decomposition at 500 °C. Therefore, chemical solution deposition was suggested as a suitable deposition method to evaluate the newly synthesized tin precursor for the growth of SnO and SnO_2 films. Among the various complexes, $[Sn(dmamp)(edpa)]_2$ (**6**) exhibited the most suitable characteristics for solution deposition by spin-coating. In CSD, the solubility and stability of the precursor in a selected solvent and the properties of the solvent are important to ensure a good deposition characteristic. Solvents with low boiling points tend to evaporate early during spin-coating, resulting in incomplete dispersion of the precursor solution and film inhomogeneity.[48] Among the solvents tested, toluene exhibited the most favorable conditions in terms of precursor solubility and boiling point (111 °C). Thus, using toluene as solvent, the complex **6** solution (0.05 M) was spin-coated onto SiO_2 and a sodalime glass substrate. The coated substrates were then dried at 110 °C for 10 min to remove residual toluene. In the subsequent PDA process, the films were preheated at 300 °C for 15 min under either argon and oxygen flow at 50 Torr followed by further heating to 500 °C for 1 h at the same pressure.

https://doi.org/10.1021/acsomega.1c05744
ACS Omega 2022, 7, 1232−1243

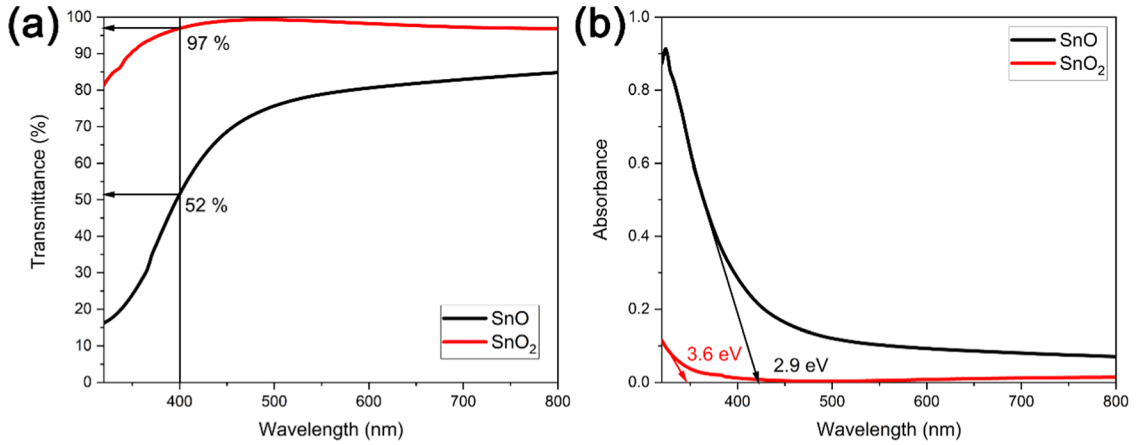

Figure 9. UV−visible (a) transmittance and (b) absorbance spectra for SnO and SnO_2 films.

The crystallinity of the deposited films after PDA was investigated by high-resolution GAXRD. Figure 7a,b shows the diffraction patterns of the deposited films annealed under argon and oxygen ambient, respectively. The SnO_x film annealed under argon ambient exhibited very high crystallinity with diffraction peaks detected at 29.9, 33.4, 37.1, 48.0, 50.8, 57.6, and 62.6°, corresponding to the (101), (110), (002), (200), (112), (211), and (103) planes of tetragonal romarchite SnO. (PDF No:04-008-7670, JCPDS). It should be noted that only SnO diffraction peaks were observed without the SnO_2 phase. The deposited SnO films exhibited a preferential growth orientation along the (101) direction. By contrast, the films annealed in oxygen ambient displayed diffraction peaks at 26.9, 34.2, 38.2, and 52.1°, corresponding to the (110), (101), (200), and (211) planes of tetragonal cassiterite SnO_2 (PDF No:04-012-0770, JCPDS) as depicted in Figure 7b. The formation of only the SnO_2 phase rather than SnO might be ascribed to complete oxidation of the Sn^{2+} cation in complex **6** to Sn^{4+} as a result of high-temperature PDA in oxidizing ambient. The SnO_2 film showed less degree of crystallinity compared to the SnO film, which can be understood from a small grain size as presented later in the field emission scanning electron microscope (FE-SEM) image.

The FE-SEM plane and cross-sectional images of the SnO film on the SiO_2 substrate are illustrated in Figure 8a,b. The SnO film was characterized by very small, agglomerated grains with noticeable pores. The nanopores are suspected to be generated by the evaporation of the Sn metal during PDA in argon ambient at a high temperature of 500 °C. Becker et al. studied tin oxide of different stoichiometries synthesized under variable oxygen pressure and temperature conditions, where a mixture of Sn metal and SnO were obtained between 200 and 500 °C, and low oxygen pressure.[49] Figure 8c,d shows the plane and cross-sectional images of the SnO_2 film on a SiO_2 substrate. Highly dense and pin-hole-free SnO_2 films were prepared in contrast to the SnO film. The thickness of each film was found to be 147 nm each in cross-sectional images.

UV−visible spectroscopy was used to determine the optical properties of the prepared SnO_x films. The transmittance and absorbance spectra of the films were measured in the wavelength range of 350−800 nm. As shown in Figure 9a, the SnO_2 films exhibited a high transmittance of >97% in the visible region (400−700 nm), whereas the SnO films demonstrated a comparatively lower transmittance of >52%. This might be explained by the difference in the optical band gap of SnO_2 and SnO films. From the absorbance spectra in Figure 9b, an optical band gap of 2.9 eV was estimated for the SnO films while the SnO_2 films exhibited a wider band gap of 3.6 eV, which was visually evident from the growth of brown films for SnO and colorless transparent films for SnO_2. The estimated values are in good agreement with previously reported optical direct band gap values of 2.5−3.4 eV (SnO)[50] and 3.6 eV (SnO_2),[51] and further support the selective growth of SnO and SnO_2 films using complex **6**.[52]

The chemical composition and residual impurities of the SnO_x films were investigated by XPS. XPS atomic percent of SnO and SnO_2 films are listed in Table 4. Figure 10a shows the

Table 4. Atomic Percent in XPS of SnO and SnO_2 Thin Films

	SnO	SnO_2
C	25.1	2.2
N	2.0	1.1
Sn	39.6	44.3
O	33.3	52.3
O/Sn	0.9	1.2

Sn 3d spectra of the SnO_x films annealed in argon or O_2 ambient. After PDA in argon ambient, the Sn $3d_{5/2}$ peak is positioned at 486.2 eV, confirming an oxidation state of +2. This finding is consistent with the previous results from XRD and UV−visible spectra. For PDA in oxygen ambient, the Sn $3d_{5/2}$ peak is shifted to higher binding energy, and centered at 486.5 eV corresponding to the Sn oxidation state of +4, indicating the formation of the SnO_2 film rather than the SnO phase. The Sn $3d_{5/2}$ peak corresponding to the oxidation state of +2 (~486.2 eV) was not observed, implying that the oxidation of the Sn^{2+} cation in complex **6** is Sn^{4+} during PDA in O_2 ambient. For the O 1s spectra of SnO_x films, peaks centered at 530.2 and 530.5 eV for SnO and SnO_2 films are observed, respectively, as shown in Figure 10b. This is consistent with the reported peak positions of O 1s peaks for SnO and SnO_2 phases.[53] C 1s and N 1s spectra were investigated to examine the residual carbon and nitrogen in SnO_x films after PDA. As shown in Figure 10c, no carbon was detected in the SnO_2 films after PDA in oxygen ambient, which indicates complete removal of organic ligands in complex **6**. On the other hand, there are significant carbon residues in the SnO film, which is annealed in argon ambient, due to the

https://doi.org/10.1021/acsomega.1c05744
ACS Omega 2022, 7, 1232−1243

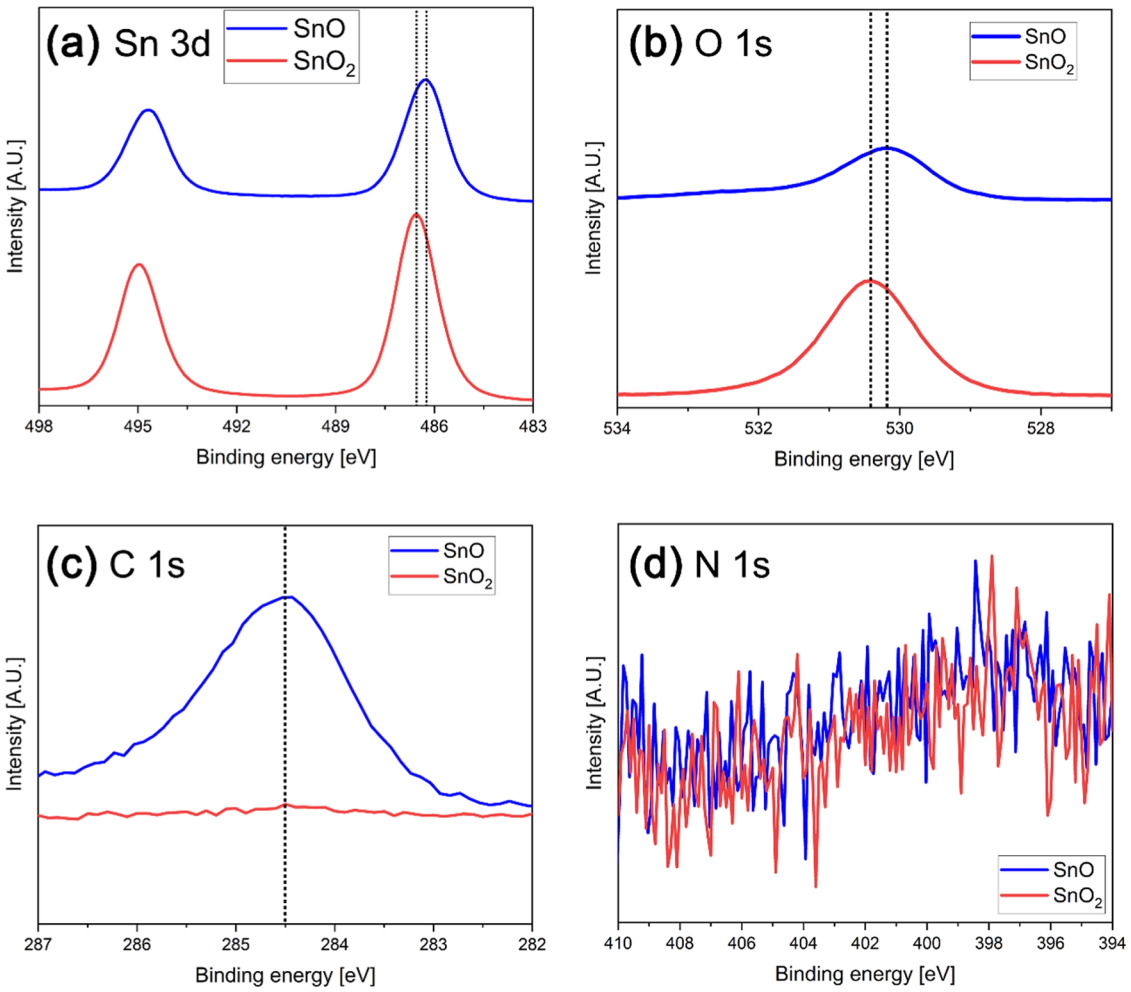

Figure 10. XP spectra of SnO and SnO_2 films after PDA at 500 °C (a) Sn 3d spectra, (b) O 1s spectra, and (c) C 1s spectra of SnO and SnO_2 films after surface etching, and (d) N 1s spectra of SnO and SnO_2 films after surface etching.

incorporation of carbon into the SnO film after decomposition of ligand species during PDA. For N 1s spectra, as depicted in Figure 10d, no noticeable peak was found for both SnO and SnO_2 films, irrespective of PDA ambient. Nitrogen concentration below the detection level in all SnO_x films may indicate the preferential removal of the nitrogen-containing dmamp ligand over the edpa ligand during PDA in argon. The SnO film exhibited an average O/Sn ratio of 0.9 and the SnO_2 film showed an average O/Sn ratio of 1.2. It is worth noting that the absolute O/Sn ratio determined by XPS quantitative analysis is not very accurate even with the consideration of atomic sensitivity factors.[27]

CONCLUSIONS

We successfully synthesized new heteroleptic tin complexes using aminoalkoxide (dmamp) and various *N*-alkoxy carboxamide (empa, mdpa, and edpa) ligands via controlled salt metathesis reactions. All complexes were obtained as dimers in their crystal structures through single-crystal X-ray diffraction analysis. The alkoxy oxygen of the dmamp functioned as a bridge between each tin metal via μ_2−O bonding. Complexes **1**−**5** exhibited distorted trigonal bipyramidal geometries around tin metal centers with lone pair electrons on tin. The TGA curves of **4**−**6** displayed multistep weight loss owing to their thermal instability. Compound **6** was successfully evaluated as a tin precursor to selectively deposit SnO and SnO_2 films by CSD depending on the PDA atmospheres of argon and oxygen. The SnO and SnO_2 films exhibited good crystallinity with tetragonal romarchite and tetragonal cassiterite structures, respectively. The SnO_2 films exhibited a high transmittance of >97% in the visible range and a band gap of 3.6 eV, while the SnO films showed a lower transmittance of >52% and a band gap of 2.9 eV, although carbon impurities were incorporated into them. This study showed the feasibility of newly synthesized tin precursors for selective growth of SnO and SnO_2 films, and further opens the door for their potential applications in TFTs and photovoltaics.

EXPERIMENTAL

Materials. ^{1}H and the proton-decoupled ^{13}C NMR spectra were recorded on a Bruker Advance NEO 500 MHz spectrometer with C_6D_6 as the solvent and standard. The proton-decoupled ^{119}Sn NMR spectra were recorded on a Bruker Liquid 400 MHz NMR spectrometer with $CDCl_3$ as the solvent and standard. FT-IR spectra were obtained using a Nicolet Nexus FT-IR spectrophotometer with a 4 mm KBr window or KBr pellets. The KBr pellets for the samples were prepared by a standard pellet technique inside an argon-filled glovebox. The elemental analyses were performed with a Thermo Scientific FLASH EA-2000 Organic elemental

https://doi.org/10.1021/acsomega.1c05744
ACS Omega 2022, 7, 1232−1243

analyzer. The melting point analyses were performed using a Stuart SMP40 Automatic Melting Point apparatus with 100 mm-length capillaries. The capillaries for the samples were prepared inside an argon-filled glovebox. Thermogravimetric analyses were conducted on a Thermo plus EVO II TG8120 series thermogravimetry and differential thermal analysis instrument under a constant flow of nitrogen. All reactions, except for the ligand preparations, were performed under inert and dry conditions using standard Schlenk techniques or in an argon-filled glovebox. The dmampH was synthesized by a slightly modified literature method.[54,55] Na(dmamp) was prepared by the reaction of dmampH and sodium metal in hexane. The series of *N*-alkoxycarboxamidate (mdpaH, edpaH, empaH) were synthesized by the literature method.[47] Na(*N*-alkoxycarboxamidate) were prepared by the reaction of *N*-alkoxycarboxamidate and sodium hydride in THF. Hexane, toluene, and THF were purified using an Innovative Technology PS−MD−4 solvent purification system. Tin halides ($SnCl_2$, $SnBr_2$, SnI_2) were purchased from Strem Chemicals, pivaloyl chloride was purchased from Sigma Aldrich, and all other chemicals were purchased from TCI and used as received.

General Procedure for the Synthesis of [XSn(dmamp)]$_2$ Complexes. A THF solution (10 mL) of Na(dmamp) was added dropwise to a solution of SnX_2 in THF (50 mL) at room temperature with constant stirring under inert gas conditions for 15 h. After completion of the reaction, the mixture was filtered and dried to obtain the product. The pure product was obtained by recrystallization from THF. X-ray quality crystals were grown by slow evaporation from a saturated THF solution in a glovebox at room temperature.

*[ClSn(dmamp)]$_2$ (**1**).* $SnCl_2$ (0.190 g, 1 mmol) and Na(dmamp) (0.139 g, 1 mmol) were used. White crystals were obtained. Yield: 0.22 g (81%). M.P. 190 °C. FT-IR (KBr, cm^{-1}): 3029(w), 2961(s), 2867(s), 2801(m), 1459(s), 1403(m), 1386(m), 1360(s), 1306(s), 1252(m), 1236(m), 1211(s), 1184(s), 1144(s), 1122(s), 1091(m), 1030(s), 978(s), 932(s), 908(s), 836(s), 783(s), 622(s), 509(s), 452(s). ^{1}H NMR (C_6D_6, 500 MHz): δ = 1.49 (6H, br, $SnOC(CH_3)_2$), 1.79 (3H, s, $SnN(CH_3)_2$), 1.92 (1H, s, $SnN(CH_3)_2CH_2$), 2.20 (3H, s, $SnN(CH_3)_2$), 2.49 (1H, s, $SnN(CH_3)_2CH_2$) ppm. ^{13}C{^{1}H} NMR (C_6D_6, 125.8 MHz): δ = 32.9 ($SnOC(CH_3)_2$), 45.9 ($SnN(CH_3)_2$), 47.1 ($SnN(CH_3)_2$), 70.9 ($SnOC(CH_3)_2$), 75.9 ($SnN(CH_3)_2CH_2$) ppm. Anal. Calcd for $C_{12}H_{28}N_2O_2Cl_2Sn_2$: C, 26.7; H, 5.22; N, 5.18. Found: C, 27.2; H, 5.33; N, 4.79.

*[BrSn(dmamp)]$_2$ (**2**).* $SnBr_2$ (0.278 g, 1 mmol) and Na(dmamp) (0.139 g, 1 mmol) were used. White crystals were obtained. Yield: 0.25 g (79%). FT-IR (KBr, cm^{-1}): 2962(s), 2864(s), 2799(m), 1460(s), 1409(m), 1397(m), 1361(s), 1301(m), 1250(w), 1237(w), 1208(s), 1183(s), 1141(s), 1124(s), 1030(s), 1015(m), 979(s), 928(s), 908(s), 831(s), 782(s), 620(s), 509(s), 483(w), 433(s). ^{1}H NMR (C_6D_6, 500 MHz): δ = 1.49 (6H, s, $SnOC(CH_3)_2CH_2$), 2.01 (6H, s, $SnN(CH_3)_2CH_2$), 2.24 (2H, s, $SnN(CH_3)_2CH_2$) ppm. ^{13}C{^{1}H} NMR (C_6D_6, 125.8 MHz): δ = 32.7 ($SnOC(CH_3)_2$), 46.3 ($SnN(CH_3)_2$), 70.9 ($SnOC(CH_3)_2$), 76.3 ($SnN(CH_3)_2CH_2$) ppm. Anal. Calcd for $C_{12}H_{28}N_2O_2Br_2Sn_2$: C, 22.9; H, 4.48; N, 4.45. Found: C, 22.6; H, 4.56; N, 4.33.

*[ISn(dmamp)]$_2$ (**3**).* SnI_2 (0.373 g, 1 mmol) and Na(dmamp) (0.139 g, 1 mmol) were used. White crystals were obtained. Yield: 0.27 g (75%). FT-IR (KBr, cm^{-1}): 2986(m), 2958(s), 2857(s), 1470(s), 1455(s), 1402(s), 1387(s), 1373(s), 1361(s), 1298(m), 1254(w), 1210(s), 1181(s), 1139(s), 1127(s), 1024(s), 974(s), 927(s), 902(s), 829(s), 785(s), 623(s), 513(s), 467(s). ^{1}H NMR (C_6D_6, 500 MHz): δ = 1.47 (6H, s, $SnOC(CH_3)_2$), 2.05 (6H, s, $SnN(CH_3)_2$), 2.31 (2H, br, $SnN(CH_3)_2CH_2$) ppm. ^{13}C{^{1}H} NMR (C_6D_6, 125.8 MHz): δ = 32.2 ($SnOC(CH_3)_2$), 46.1 ($SnN(CH_3)_2$), 71.0 ($SnOC(CH_3)_2$) ppm. Anal. Calcd for $C_{12}H_{28}N_2O_2I_2Sn_2$: C, 19.9; H, 3.90; N, 3.87. Found: C, 20.2; H, 3.97; N, 3.87.

*General Procedure for the Synthesis of [Sn(dmamp)(*N*-alkoxycarboxamidate)]$_2$ Complexes.* A THF solution (10 mL) of the corresponding sodium carboxamidate was added dropwise to a solution of [BrSn(dmamp)]$_2$ in THF (50 mL) at room temperature with constant stirring under inert gas conditions for 15 h. After the reaction was complete, volatiles was removed in vacuo, and the residue was extracted into hexane and filtered. The hexane was then removed to obtain the crude product. X-ray quality crystals were grown by slow evaporation from a saturated hexane solution in a glovebox at room temperature.

*[Sn(dmamp)(empa)]$_2$ (**4**).* [BrSn(dmamp)]$_2$ (**2**) (0.314 g, 0.5 mmol) and Na(empa) (0.167 g, 1 mmol) were used. The crude product was recrystallized to obtain the pure product as white crystals. Yield: 0.25 g (69%). M.P. 95 °C. FT-IR (KBr, cm^{-1}): 2963(s), 2866(s), 1600(s), 1469(s), 1382(s), 1345(s), 1302(m), 1277(s), 1211(m), 1185(w), 1137(s), 1079(s), 1054(s), 975(s), 924(s), 836(m), 784(s), 729(w), 664(m), 620(s), 542(w), 502(m). ^{1}H NMR (C_6D_6, 500 MHz): δ = 1.35 (9H, br m, $SnO(CH_2CH_3)N = C(CH(CH_3)_2)O$), 1.44 (6H, br, $SnOC(CH_3)_2$), 2.06 (6H, s, $SnN(CH_3)_2$), 2.20 (2H, br, $SnN(CH_3)_2CH_2$), 2.81 (1H, br, $SnOCCH(CH_3)_2$), 4.18 (2H, q, $SnOCH_2CH_3$) ppm. ^{13}C{^{1}H} NMR (C_6D_6, 125.8 MHz): δ = 15.8 ($SnO(CH_2CH_3)$), 21.1 ($SnOCCH(CH_3)_2$), 32.7 ($SnOCCH(CH_3)_2$), 33.2 ($SnOC(CH_3)_2$), 46.4 ($SnN(CH_3)_2$), 67.9 ($SnOCH_2CH_3$), 71.7 ($SnOC(CH_3)_2$), 74.2 ($SnN(CH_3)_2CH_2$) ppm. ^{119}Sn{^{1}H} NMR ($CDCl_3$, 149.2 MHz): δ = −418.2 ppm. Anal. Calcd for $C_{24}H_{52}N_4O_6Sn_2$: C, 39.5; H, 7.18; N, 7.67. Found: C, 38.9; H, 7.19; N, 7.87.

*[Sn(dmamp)(mdpa)]$_2$ (**5**).* [BrSn(dmamp)]$_2$ (**2**) (0.314 g, 0.5 mmol) and Na(mdpa) (0.167 g, 1 mmol) were used. The crude product was recrystallized to obtain the pure product as white crystals. Yield: 0.28 g (78%). M.P. 137 °C. FT-IR (KBr, cm^{-1}): 2966(s), 1725(w), 1581(s), 1479(s), 1388(s), 1358(s), 1327(s), 1202(s), 1145(s), 1068(s), 980(s), 933(s), 904(s), 864(s), 834(s), 788(s), 734(m), 619(s), 504(s). ^{1}H NMR (C_6D_6, 500 MHz): δ = 1.43 (6H, s, $SnOC(CH_3)_2$), 1.48 (9H, s, $SnOCC(CH_3)_3$), 2.02 (6H, s, $SnN(CH_3)_2$), 2.21 (2H, s, $SnN(CH_3)_2CH_2$), 3.82 (3H, s, $SnOCH_3$) ppm. ^{13}C{^{1}H} NMR (C_6D_6, 125.8 MHz): δ = 29.0 ($SnOCC(CH_3)_3$), 33.1 ($SnOC(CH_3)_2$), 36.6 ($SnOCC(CH_3)_3$), 46.3 ($SnN(CH_3)_2$), 59.3 ($SnOCH_3$), 71.5 ($SnOC(CH_3)_2$), 74.5 ($SnN(CH_3)_2CH_2$), 169.0 (SnOC = N) ppm. ^{119}Sn{^{1}H} NMR ($CDCl_3$, 149.2 MHz): δ = −414.4 ppm. Anal. Calcd for $C_{24}H_{52}N_4O_6Sn_2$: C, 39.5; H, 7.18; N, 7.67. Found: C, 39.0; H, 7.23; N, 7.04.

*[Sn(dmamp)(edpa)]$_2$ (**6**).* [BrSn(dmamp)]$_2$ (**2**) (0.314 g, 0.5 mmol) and Na(edpa) (0.167 g, 1 mmol) were used. The crude product was recrystallized to obtain the pure product as white crystals. Yield: 0.30 g (79%). M.P. 115 °C. FT-IR (KBr, cm^{-1}): 2968(s), 1586(s), 1481(s), 1388(s), 1360(s), 1326(s), 1257(m), 1202(s), 1134(s), 1092(m), 1055(s), 979(m), 964(m), 923(s), 866(m), 834(m), 787(s), 732(w), 620(s), 600(s), 564(w), 503(m). ^{1}H NMR (C_6D_6, 500 MHz): δ = 1.32 (3H, br, $SnOCH_2CH_3$), 1.42 (6H, br, $SnOC(CH_3)_2$),

https://doi.org/10.1021/acsomega.1c05744
ACS Omega 2022, 7, 1232−1243

1.46 (9H, br, $SnOCC(CH_3)_3$), 2.05 (6H, s, $SnN(CH_3)_2CH_2$), 2.21 (2H, br, $SnN(CH_3)_2CH_2$), 4.16 (2H, q, $SnOCH_2CH_3$) ppm. $^{13}C\{^1H\}$ NMR (C_6D_6, 125.8 MHz): δ = 15.9 ($SnO(CH_2CH_3)$), 29.1 ($SnOCC(CH_3)_3$), 33.2 ($SnOC(CH_3)_2$), 36.8 ($SnOCC(CH_3)_3$), 46.4 ($SnN(CH_3)_2$), 67.9 ($SnOCH_2CH_3$), 71.6 ($SnOC(CH_3)_2$), 74.2 ($SnN(CH_3)_2CH_2$), 168.3 (SnOC = N) ppm. $^{119}Sn\{^1H\}$ NMR ($CDCl_3$, 149.2 MHz): δ = −417.2 ppm. Anal. Calcd for $C_{26}H_{56}N_4O_6Sn_2$: C, 41.2; H, 7.45; N, 7.39. Found: C, 40.6; H, 7.43; N, 7.04.

Crystallography. Single crystals of **1**−**3** were grown by slow evaporation from a saturated THF solution in a glovebox at room temperature, and single crystals of **4**−**5** were grown from a saturated hexane solution at −30 °C. The as-obtained specimen of suitable size and quality was coated with Paratone oil and mounted on a glass capillary. Reflection data were collected using a Bruker SMART Apex II CCD area detector diffractometer with graphite-monochromated Mo Kα radiation (λ = 0.71073 Å). The hemisphere of the reflection data was collected as ω-scan frames with 0.3° per frame and an exposure time of 10 s per frame. The cell parameters were determined and refined using the SMART program.[56] The data reduction was performed using SAINT software.[57] The data were corrected for Lorentz and polarization effects and an empirical absorption correction was applied using the SADABS program.[58] The structures of the prepared compounds were solved by direct methods and all nonhydrogen atoms were subjected to anisotropic refinement by the full-matrix least-squares method on F2 using the SHELXTL/PC package.[59] Hydrogen atoms were placed at their geometrically calculated positions and refined based on the corresponding carbon atoms with isotropic thermal parameters.

The supplementary crystallographic data for this paper can be found in CCDC 1998673 (**1**), 1998674 (**2**), 1998675 (**3**), 1998676 (**4**), and 1998677 (**5**). These data can be obtained free of charge from The Cambridge Crystallographic Data Centre.

Deposition and Characterization of SnO_x Thin Films. The 0.05 M solution of $[Sn(dmamp)(edpa)]_2$ (**6**) in toluene was used for spin-coating of SnO_x thin films on OH-terminated SiO_2 (300 nm)/Si and glass substrates. Spin-coating was performed at room temperature in an argon-filled glovebox. The solution was dispensed onto the substrates and allowed to sit for 60 s after which the spinning speed was increased to 1000 rpm for 10 s, 2000 rpm for 10 s, and then to 3000 rpm for 30 s. After coating, the samples were immediately annealed at 110 °C for 10 min to remove the solvent. This process was repeated 10 times to prepare thick films. Thereafter, PDA was conducted to selectively obtain SnO and SnO_2 phases. The SnO films were achieved by PDA at 300 °C for 15 min in argon ambient at 50 Torr and subsequent PDA at 500 °C for 1 h at the same pressure. By contrast, the SnO_2 films were achieved by PDA at 300 °C for 15 min in O_2 ambient at 50 Torr and subsequent PDA at 500 °C for 1 h at the same pressure.

The film coating was performed using a spin coater (SPIN-1200D, Midas-System). Post-deposition annealing was carried out using a vacuum furnace (PDA, S&R). The film crystallinity was investigated via glancing angle X-ray diffraction (GAXRD, Smart-Lab, Rigaku). An X-ray photoelectron spectrometer (XPS, K-Alpha, Thermo Scientific) equipped with a monochromatic Al Kα X-ray source was used to determine the chemical composition and impurities in the films. All XP spectra were obtained after surface sputtering using Ar ions, and were calibrated according to the C−C bonding peak at 284.6 eV. As the optical transparency of the SnO_x films is of importance for transparent device application, the transmittance and absorbance of the deposited films on sodalime glass substrates were determined using a UV−visible spectrometer (UV-2550, Shimadzu). Finally, the surface morphologies of the films were investigated using a field emission scanning electron microscope (FE-SEM, LSM 880, Carl Zeiss).

■ ASSOCIATED CONTENT

Supporting Information

The Supporting Information is available free of charge at https://pubs.acs.org/doi/10.1021/acsomega.1c05744.

$[ClSn(dmamp)]_2$ (CIF)
$[BrSn(dmamp)]_2$ (CIF)
$[ISn(dmamp)]_2$ (CIF)
$[Sn(dmamp)(empa)]_2$ (CIF)
$[Sn(dmamp)(mdpa)]_2$ (CIF)

Accession Codes

CCDC 1998673-1998677 contain the supplementary crystallographic data for this paper. These data can be obtained free of charge via www.ccdc.cam.ac.uk/data_request/cif, or by emailing data_request@ccdc.cam.ac.uk, or by contacting The Cambridge Crystallographic Data Centre, 12 Union Road, Cambridge CB2 1EZ, U.K.; fax: +44 1223 336033.

■ AUTHOR INFORMATION

Corresponding Author

Taek-Mo Chung − *Thin Film Materials Research Center, Korea Research Institute of Chemical Technology, Daejeon 34114, Republic of Korea; Department of Advanced Materials and Chemical Engineering, University of Science and Technology (UST), Daejeon 34113, Republic of Korea;* orcid.org/0000-0002-5169-2671; Phone: +82-42-860-7359; Email: tmchung@krict.re.kr

Authors

Seong Ho Han − *Thin Film Materials Research Center, Korea Research Institute of Chemical Technology, Daejeon 34114, Republic of Korea; Department of Chemistry and Department of Energy Science, Sungkyunkwan University, Suwon-si, Gyeonggi-do 16419, Republic of Korea;* orcid.org/0000-0001-5360-7453

Raphael Edem Agbenyeke − *Thin Film Materials Research Center, Korea Research Institute of Chemical Technology, Daejeon 34114, Republic of Korea; Department of Advanced Materials and Chemical Engineering, University of Science and Technology (UST), Daejeon 34113, Republic of Korea*

Ga Yeon Lee − *Thin Film Materials Research Center, Korea Research Institute of Chemical Technology, Daejeon 34114, Republic of Korea; Department of Chemistry and Department of Energy Science, Sungkyunkwan University, Suwon-si, Gyeonggi-do 16419, Republic of Korea*

Bo Keun Park − *Thin Film Materials Research Center, Korea Research Institute of Chemical Technology, Daejeon 34114, Republic of Korea; Department of Advanced Materials and Chemical Engineering, University of Science and Technology (UST), Daejeon 34113, Republic of Korea;* orcid.org/0000-0002-4066-0500

Chang Gyoun Kim − *Thin Film Materials Research Center, Korea Research Institute of Chemical Technology, Daejeon*

https://doi.org/10.1021/acsomega.1c05744
ACS Omega 2022, 7, 1232−1243

34114, Republic of Korea; Department of Advanced Materials and Chemical Engineering, University of Science and Technology (UST), Daejeon 34113, Republic of Korea

Taeyong Eom − *Thin Film Materials Research Center, Korea Research Institute of Chemical Technology, Daejeon 34114, Republic of Korea;* orcid.org/0000-0002-9646-9553

Seung Uk Son − *Department of Chemistry and Department of Energy Science, Sungkyunkwan University, Suwon-si, Gyeonggi-do 16419, Republic of Korea;* orcid.org/0000-0002-4779-9302

Jeong Hwan Han − *Department of Materials Science and Engineering, Seoul National University of Science and Technology, Seoul 01811, Republic of Korea;* orcid.org/0000-0002-8314-9235

Ji Yeon Ryu − *Thin Film Materials Research Center, Korea Research Institute of Chemical Technology, Daejeon 34114, Republic of Korea;* orcid.org/0000-0001-6321-5576

Complete contact information is available at: https://pubs.acs.org/10.1021/acsomega.1c05744

Notes

The authors declare no competing financial interest.

■ ACKNOWLEDGMENTS

This research was supported by a grant for the development of smart chemical materials for IoT devices project through the Korea Research Institute of Chemical Technology (KRICT) of the Republic of Korea (SS2121-10), the Nano Material Technology Development Program (Green Nano Technology Program) through the National Research Foundation ok Korea (NRF) funded by the Ministry of Science and ICT (2020M3A7B4026383), and the National R&D Program through the National Research Foundation of Korea(NRF) funded by the Ministry of Science and ICT(2020M3-H4A3081866).

■ REFERENCES

(1) Kucheyev, S. O.; Baumann, T. F.; Sterne, P. A.; Wang, Y. M.; van Buuren, T.; Hamza, A. V.; Terminello, L. J.; Willey, T. M. Surface electronic states in three-dimensional SnO_2 nanostructures. *Phys. Rev. B* **2005**, *72*, No. 035404.

(2) Jarzebski, Z. M.; Marton, J. P. Physical Properties of SnO_2 Materials. *J. Electrochem. Soc.* **1976**, *123*, 299C.

(3) Isono, T.; Fukuda, T.; Nakagawa, K.; Usui, R.; Satoh, R.; Morinaga, E.; Mihara, Y. Highly conductive SnO_2 thin films for flat-panel displays. *J. Soc. Inf. Disp.* **2007**, *15*, 161−166.

(4) Godinho, K. G.; Walsh, A.; Watson, G. W. Energetic and Electronic Structure Analysis of Intrinsic Defects in SnO_2. *J. Phys. Chem. C* **2009**, *113*, 439−448.

(5) Reti, F.; Kiss, G.; Perczel, I. V. Subjective Overview on Oxide Semiconductor Gas Sensors. *Sens. Mater.* **2004**, *16*, 53−69.

(6) Pandey, P. C.; Upadhyay, B. C.; Pandey, C. M. D.; Pathak, H. C. Electrochemical studies on D96N bacteriorhodopsin and its application in the development of photosensors. *Sens. Actuators, B* **1999**, *56*, 112−120.

(7) Wang, W.-W.; Zhu, Y.-J.; Yang, L.-X. ZnO−SnO_2 Hollow Spheres and Hierarchical Nanosheets: Hydrothermal Preparation, Formation Mechanism, and Photocatalytic Properties. *Adv. Funct. Mater.* **2007**, *17*, 59−64.

(8) Harrison, P. G.; Willett, M. J. The mechanism of operation of tin(IV) oxide carbon monoxide sensors. *Nature* **1988**, *332*, 337−339.

(9) Wang, Y.; Jiang, X.; Xia, Y. A Solution-Phase, Precursor Route to Polycrystalline SnO_2 Nanowires That Can Be Used for Gas Sensing under Ambient Conditions. *J. Am. Chem. Soc.* **2003**, *125*, 16176−16177.

(10) Singkammo, S.; Wisitsoraat, A.; Sriprachuabwong, C.; Tuantranont, A.; Phanichphant, S.; Liewhiran, C. Electrolytically Exfoliated Graphene-Loaded Flame-Made Ni-Doped SnO_2 Composite Film for Acetone Sensing. *ACS Appl. Mater. Interfaces* **2015**, *7*, 3077−3092.

(11) Gordon, R. Chemical vapor deposition of coatings on glass. *J. Non-Cryst. Solids* **1997**, *218*, 81−91.

(12) Yu, X.; Marks, T. J.; Facchetti, A. Metal oxides for optoelectronic applications. *Nat. Mater.* **2016**, *15*, 383−396.

(13) Bradshaw, G.; Hughes, A. J. Etching methods for indium oxide/tin oxide films. *Thin Solid Films* **1976**, *33*, L5−L7.

(14) Caraveo-Frescas, J. A.; Nayak, P. K.; Al-Jawhari, H. A.; Granato, D. B.; Schwingenschlögl, U.; Alshareef, H. N. Record Mobility in Transparent p-Type Tin Monoxide Films and Devices by Phase Engineering. *ACS Nano* **2013**, *7*, 5160−5167.

(15) Khandelwal, R.; Singh, A. P.; Kapoor, A.; Grigorescu, S.; Miglietta, P.; Stankova, N. E.; Perrone, A. Effects of deposition temperature on the structural and morphological properties of SnO_2 films fabricated by pulsed laser deposition. *Opt. Laser Technol.* **2009**, *41*, 89−93.

(16) Ma, J.; Hao, X.; Ma, H.; Xu, X.; Yang, Y.; Huang, S.; Zhang, D.; Cheng, C. RF magnetron sputtering SnO_2: Sb films deposited on organic substrates. *Solid State Commun.* **2002**, *121*, 345−349.

(17) Minami, T.; Kakumu, T.; Shimokawa, K.; Takata, S. New transparent conducting ZnO−In_2O_3−SnO_2 thin films prepared by magnetron sputtering. *Thin Solid Films* **1998**, *317*, 318−321.

(18) Madhusudhana Reddy, M. H.; Jawalekar, S. R.; Chandorkar, A. N. The effect of heat treatment on the structural properties of electron-beam-evaporated SnO_2 films. *Thin Solid Films* **1989**, *169*, 117−126.

(19) Barbul, I.; Johnson, A. L.; Kociok-Köhn, G.; Molloy, K. C.; Silvestru, C.; Sudlow, A. L. The Reaction and Materials Chemistry of $[Sn_6(O)_4(OSiMe_3)_4]$: Chemical Vapour Deposition of Tin Oxide. *ChemPlusChem* **2013**, *78*, 866−874.

(20) Hill, M. S.; Johnson, A. L.; Lowe, J. P.; Molloy, K. C.; Parish, J. D.; Wildsmith, T.; Kingsley, A. L. Aerosol-assisted CVD of SnO from stannous alkoxide precursors. *Dalton Trans.* **2016**, *45*, 18252−18258.

(21) Khanderi, J.; Davaasuren, B.; Alshankiti, B. A.; Rothenberger, A. Tin(II) ketoacidoximates: synthesis, X-ray structures and processing to tin(II) oxide. *Dalton Trans.* **2015**, *44*, 19820−19828.

(22) Wildsmith, T.; Hill, M. S.; Johnson, A. L.; Kingsley, A. J.; Molloy, K. C. Exclusive formation of SnO by low temperature single-source AACVD. *Chem. Commun.* **2013**, *49*, 8773−8775.

(23) George, S. M. Atomic Layer Deposition: An Overview. *Chem. Rev.* **2010**, *110*, 111−131.

(24) Mullings, M. N.; Hägglund, C.; Bent, S. F. Tin oxide atomic layer deposition from tetrakis(dimethylamino)tin and water. *J. Vac. Sci. Technol., A* **2013**, *31*, No. 061503.

(25) Schwartz, R. W. Chemical Solution Deposition of Perovskite Thin Films. *Chem. Mater.* **1997**, *9*, 2325−2340.

(26) Ansari, S. G.; Dar, M. A.; Dhage, M. S.; Kim, Y. S.; Ansari, Z. A.; Al-Hajry, A.; Shin, H.-S. A novel method for preparing stoichiometric SnO_2 thin films at low temperature. *Rev. Sci. Instrum.* **2009**, *80*, No. 045112.

(27) Kim, H. Y.; Nam, J. H.; George, S. M.; Park, J.-S.; Park, B. K.; Kim, G. H.; Jeon, D. J.; Chung, T.-M.; Han, J. H. Phase-controlled SnO_2 and SnO growth by atomic layer deposition using Bis(N-ethoxy-2,2-dimethyl propanamido)tin precursor. *Ceram. Int.* **2019**, *45*, 5124−5132.

(28) Félix, R.; Llobera-Vila, N.; Hartmann, C.; Klimm, C.; Hartig, M.; Wilks, R. G.; Bär, M. Preparation and in-system study of $SnCl_2$ precursor layers: towards vacuum-based synthesis of Pb-free perovskites. *RSC Adv.* **2018**, *8*, 67−73.

(29) Heo, J.; Kim, S. B.; Gordon, R. G. Atomic layer deposition of tin oxide with nitric oxide as an oxidant gas. *J. Mater. Chem.* **2012**, *22*, 4599−4602.

(30) Han, J. H.; Chung, Y. J.; Park, B. K.; Kim, S. K.; Kim, H.-S.; Kim, C. G.; Chung, T.-M. Growth of p-Type Tin(II) Monoxide Thin

Films by Atomic Layer Deposition from Bis(1-dimethylamino-2-methyl-2propoxy)tin and H_2O. *Chem. Mater.* **2014**, *26*, 6088−6091.
(31) Drevet, R.; Legros, C.; Bérardan, D.; Ribot, P.; Dragoé, D.; Cannizzo, C.; Barthés-Labrousse, M. G.; Chaussé, A.; Andrieux, M. Metal organic precursor effect on the properties of SnO_2 thin films deposited by MOCVD technique for electrochemical applications. *Surf. Coat. Technol.* **2015**, *271*, 234−241.
(32) Simonenko, E. P.; Simonenko, N. P.; Mokrushin, A. S.; Vasiliev, A. A.; Vlasov, I. S.; Volkov, I. A.; Maeder, T.; Sevastyanov, V. G.; Kuznetsov, N. T. Tin Acetylacetonate as a Precursor for Producing Gas-Sensing SnO_2 Thin Films. *Russ. J. Inorg. Chem.* **2018**, *63*, 851−860.
(33) Tupala, J.; Kemell, M.; Mattinen, M.; Meinander, K.; Seppälä, S.; Hatanpää, T.; Räisänen, J.; Ritala, M.; Leskelä, M. Atomic layer deposition of tin oxide thin films from bis[bis(trimethylsilyl)amino]-tin(II) with ozone and water. *J. Vac. Sci. Technol., A* **2017**, *35*, No. 041506.
(34) Nazarov, D. V.; Bobrysheva, N. P.; Osmolovskaya, O. M.; Osmolovsky, M. G.; Smirnov, V. M. Atomic layer deposition of tin dioxide nanofilms: a review. *Rev. Adv. Mater. Sci.* **2015**, *40*, 262−275.
(35) Boyle, T. J.; Doan, T. Q.; Steele, L. A. M.; Apblett, C.; Hoppe, S. M.; Hawthorne, K.; Kalinich, R. M.; Sigmund, W. M. Tin(II) amide/alkoxide coordination compounds for production of Sn-based nanowires for lithium ion battery anode materials. *Dalton Trans.* **2012**, *41*, 9349−9364.
(36) Elinburg, J. K.; Hyre, A. S.; McNeely, J.; Alam, T. M.; Klenner, S.; Pöttgen, R.; Rheingold, A. L.; Doerrer, L. H. Formation of monomeric Sn(II) and Sn(IV) perfluoropinacolate complexes and their characterization by ^{119}Sn Mössbauer and ^{119}Sn NMR spectroscopies. *Dalton Trans.* **2020**, *49*, 13773−13785.
(37) Han, S. H.; George, S. M.; Lee, G. Y.; Han, J. H.; Park, B. K.; Kim, C. G.; Son, S. U.; Lah, M. S.; Chung, T.-M. New Heteroleptic Cobalt Precursors for Deposition of Cobalt-Based Thin Films. *ACS Omega* **2017**, *2*, 5486−5493.
(38) Kim, H.-S.; George, S. M.; Jung, E. A.; Park, B. K.; Son, S. U.; Kim, C. G.; Chung, T.-M. Heteroleptic magnesium complexes containing amidinate and aminoalkoxy ligands. *Polyhedron* **2015**, *101*, 185−190.
(39) Kim, H.-S.; George, S. M.; Park, B. K.; Son, S. U.; Kim, C. G.; Chung, T.-M. New heteroleptic magnesium complexes for MgO thin film application. *Dalton Trans.* **2015**, *44*, 2103−2109.
(40) George, S. M.; Kim, H.-S.; Park, B. K.; Kim, C. G.; Chung, T.-M. Synthesis of new heteroleptic strontium complexes stabilized by β-ketoiminato ligands. *Inorg. Chim. Acta* **2015**, *436*, 118−122.
(41) Han, S. H.; Agbenyeke, R. E.; Lee, G. Y.; Park, B. K.; Kim, C. G.; Lee, Y. K.; Son, S. U.; Chung, T.-M. Synthesis and characterization of novel zinc precursors for ZnO thin film deposition by atomic layer deposition. *Dalton Trans.* **2020**, *49*, 4306−4314.
(42) Jung, E. A.; George, S. M.; Han, J. H.; Park, B. K.; Son, S. U.; Kim, C. G.; Chung, T.-M. Indium complexes bearing donor-functionalized alkoxide ligands as precursors for indium oxide thin films. *J. Organomet. Chem.* **2017**, *833*, 43−49.
(43) Jung, E. A.; George, S. M.; Han, S. H.; Park, B. K.; Han, J. H.; Son, S. U.; Kim, C. G.; Chung, T.-M. Synthesis of novel tin complexes using functionalized oxime ligands. *Inorg. Chim. Acta* **2016**, *446*, 1−5.
(44) Khrustalev, V. N.; Zemlyansky, N. N.; Borisova, I. V.; Kuznetsova, M. G.; Krut'ko, E. B.; Antipin, M. Y. New stable germylenes, stannylenes, and related compounds 7. Synthesis and structures of compounds Hal—Sn—$OCH_2CH_2NMe_2$ (Hal = Cl or F). *Russ. Chem. Bull.* **2007**, *56*, 267−270.
(45) Müller, C.; Andrada, D. M.; Bischoff, I.-A.; Zimmer, M.; Huch, V.; Steinbrück, N.; Schäfer, A. Synthesis, Structure, and Bonding Analysis of Tin(II) Dihalide and Cyclopentadienyltin(II) Halide (Alkyl)(amino)carbene Complexes. *Organometallics* **2019**, *38*, 1052−1061.
(46) Suter, R.; Swidan, A.; Macdonald, C. L. B.; Burford, N.; Ferguson, M. J. Halogen and Sulfur Oxidation of Germanium and Tin Dications. *Inorg. Chem.* **2019**, *58*, 6238−6245.
(47) George, S. M.; Nam, J. H.; Lee, G. Y.; Han, J. H.; Park, B. K.; Kim, C. G.; Jeon, D. J.; Chung, T.-M. N-Alkoxy Carboxamide Stabilized Tin(II) and Germanium(II) Complexes for Thin-Film Applications. *Eur. J. Inorg. Chem.* **2016**, *2016*, 5539−5546.
(48) Huster, N.; Zanders, D.; Karle, S.; Rogalla, D.; Devi, A. Additive-free spin coating of tin oxide thin films: synthesis, characterization and evaluation of tin β-ketoiminates as a new precursor class for solution deposition processes. *Dalton Trans.* **2020**, *49*, 10755−10764.
(49) Becker, M.; Polity, A.; Klar, P. J.; Meyer, B. K. Synthesis of tin oxides SnO_{2-x} in the entire composition range (x = 0 to 1) by ion-beam sputter-deposition. *Phys. Status solidi RRL* **2015**, *9*, 326−330.
(50) Krishna, K. M.; Sharon, M.; Mishra, M. K.; Marathe, V. R. Selection of optimal mixing ratios to obtain suitable photoelectrodes from mixed semiconductors using band gap calculations. *Electrochim. Acta* **1996**, *41*, 1999−2004.
(51) Zhou, W.; Liu, Y.; Yang, Y.; Wu, P. Band Gap Engineering of SnO_2 by Epitaxial Strain: Experimental and Theoretical Investigations. *J. Phys. Chem. C* **2014**, *118*, 6448−6453.
(52) Cao, H.; Liang, L. Tin Oxide-Based Thin-Film Transistors and heir Circuits. In *Tin Oxide Materials: Synthesis, Properties, and Applications*; Elsevier Press, 2020; Vol. *50*, pp 441−476.
(53) Jadhav, H.; Suryawanshi, S.; More, M. A.; Sinha, S. Pulsed laser deposition of tin oxide thin films for field emission studies. *Appl. Surf. Sci.* **2017**, *419*, 764−769.
(54) Anwander, R.; Munck, F. C.; Priermeier, T.; Scherer, W.; Runte, O.; Herrmann, W. A. Volatile Donor-Functionalized Alkoxy Derivatives of Lutetium and Their Structural Characterization1. *Inorg. Chem.* **1997**, *36*, 3545−3552.
(55) Heydari, A.; Mehrdad, M.; Maleki, A.; Ahmadi, N. A New and Efficient Epoxide Ring Opening via Poor Nucleophiles: Indole, p-Nitroaniline, Borane and O-Trimethylsilylhydroxylamine in Lithium Perchlorate. *Synthesis* **2004**, *2004*, 1563−1565.
(56) *SMART*, version 5.0; Data Collection Software, Bruker AXS, Inc.: Madison, WI, 1998.
(57) *SAINT*, version 5.0; Data Integration Software, Bruker AXS Inc.: Madison, WI, 1998.
(58) Sheldrick, G. M. *SADABS, Program for Absorption Correction with the Bruker SMART System*; Universitat Gottingen: Germany, 1996.
(59) Sheldrick, M. *SHELXL-93: Program for the Refinement of Crystal Structures*; Universitat Gottingen: Germany, 1993.

https://doi.org/10.1021/acsomega.1c05744
ACS Omega 2022, 7, 1232−1243